



# An experimental study on thermophysical properties of nano-TiO<sub>2</sub>-enhanced phase change materials for cold climate applications

Lucrezia Ravasio<sup>1</sup> · Muhammad Aamer Hayat<sup>2</sup> · Rajnish Kaur Calay<sup>1</sup> · Raymond Riise<sup>1</sup> · Yong Chen<sup>2</sup>

Received: 9 July 2023 / Accepted: 14 December 2023 / Published online: 30 January 2024  
© The Author(s) 2024

## Abstract

In high-energy-demand regions, such as the Arctic, the building sector is focused on reducing the carbon footprint and mitigating environmental impact. To achieve this, phase change materials (PCMs) are being investigated for thermal energy storage due to their high latent heat of fusion. However, their limited applications arise from poor thermal conductivity. In addressing this issue, the research delves into the preparation and characterization of nano-PCMs. These materials, synthesized in a laboratory setting, exhibit enhanced thermal performance compared to pure PCMs, attributed to the incorporation of nanoparticles in the material composition. Therefore, in the study, three paraffins with different melting temperatures (10, 15 and 18 °C) are modified by incorporating titanium oxide at various concentrations (0.05, 0.1, 0.2 and 0.5 mass%). Thermal conductivity and latent heat capacity measurements were undertaken using a thermal conductivity measuring apparatus and differential scanning calorimetry, respectively. The aim was to evaluate the enhanced performance of the modified PCMs in comparison with pure PCMs and to assess their suitability for cold climate regions. Results showed that nanoparticle incorporation increased thermal conductivity by up to 37%, albeit with a slight reduction in latent heat capacity of up to 12%. Among the samples, RT18 exhibited the most significant improvement in thermal conductivity, while RT10 experienced a minor decrease in enthalpy values. Ultimately, RT10 was identified as the optimal PCM option for cold climates, as its phase change temperature range aligns with the outdoor temperatures in the Arctic.

**Keywords** PCMs · Nanoparticles · Energy · Sustainability · Building

## Introduction

Over the past few decades, phase change materials (PCMs) have garnered significant attention from researchers worldwide due to their potential benefits as thermal mass

components in building applications [1]. The increasing global carbon footprint resulting from population growth and escalating energy demand has prompted the building sector to seek solutions that enhance energy performance and minimize environmental impact throughout a building's life cycle. PCMs, as latent heat thermal energy storage systems, offer the capacity to store and release substantial energy within a narrow temperature range, making them versatile and suitable for both active and passive heating or cooling strategies in buildings.

Specifically, PCMs can serve as passive systems when integrated into building components such as roofs, windows, or the envelope [1]. In this capacity, they passively regulate indoor temperature in response to external conditions. Alternatively, they can function as active systems when incorporated into separate heat or cold storage modules, requiring active components such as pumps, fans, or control systems to circulate air or other heat transfer fluids. PCMs are classified as organic, inorganic, or eutectic based on their chemical composition. In the construction sector, organic PCMs

✉ Lucrezia Ravasio  
l.ravasio@uit.no

Muhammad Aamer Hayat  
m.hayat2@herts.ac.uk

Rajnish Kaur Calay  
rajnish.k.calay@uit.no

Raymond Riise  
Raymond.riise@uit.no

Yong Chen  
y.k.chen@herts.ac.uk

<sup>1</sup> Department of Building, Energy and Material Technology, UiT, The Arctic University of Norway, 8515 Narvik, Norway

<sup>2</sup> School of Physics, Engineering and Computer Science, University of Hertfordshire, Hatfield, UK

like paraffins are preferred due to their lower melting temperature range, compatibility with typical building operating temperatures, and competitive pricing compared to other PCM types [2]. Organic PCMs offer high-energy storage capacity, stability, non-toxicity, lack of segregation and non-corrosiveness [3]. However, their low thermal conductivity hinders heat transfer rates and may result in leakage during phase change, impacting storage capacity and limiting their applications [3]. To overcome these limitations, recent research has explored the combination of highly conductive nanoparticles with PCMs. Incorporating additives into the chemical structure of PCMs allows for improved thermal conductivity due to the low density and high conductivity of nanoparticles [4]. Extensive research has examined the effects of various types of nanoparticles, such as graphene, carbon nanotubes (CNTs), metals, metal oxides, metal carbides and metal nitrides, in different size ranges and concentrations on the physical properties of PCMs. Studies have consistently shown that incorporating graphene nanoparticles (GNPs) [5, 6], carbon nanofillers [7] and metal oxides [4, 8] into paraffin PCMs enhances their thermal conductivity compared to the base PCM. However, these studies have also revealed a reduction in latent heat values with increasing nanoparticle concentration compared to pure PCMs. Stability of nanoparticles within the enhanced PCM structure has also been a subject of analysis, leading to advanced studies focusing on stability measurements and improvement methods such as surfactant addition and nanoparticle surface treatment. Surfactants have generally demonstrated improved stability [9–12] in nanoparticle-PCM solutions, although the proper selection of a suitable surfactant for a specific PCM can affect performance. Surface treatment

has also proven effective in enhancing nanoparticle stability [13–15].

However, despite the considerable number of published studies, only a few have addressed the application of enhanced PCMs in cold climates, and none have been found specifically focusing on extreme cold environments like the Arctic. This study, for instance, combines three types of paraffins with low melting temperatures (10, 15 and 18 °C) with titanium oxide (TiO<sub>2</sub>) nanoparticles at various concentrations (0.05, 0.1, 0.2 and 0.5 mass%) to examine their thermophysical properties in cold climate conditions. Paraffin was selected as the base PCM due to its aforementioned benefits. The chosen paraffins with low melting temperature ranges align with the Arctic outdoor air temperature range and the desired indoor temperature typically set at 22 °C during cold months [16]. For this study, Narvik, a small town in Arctic Norway, serves as the reference city due to its outdoor air temperatures ranging from – 15 °C to 25 °C throughout the year (Fig. 1). Titanium oxide was selected as the nanoparticle for this investigation because, as indicated by the literature mentioned earlier, it provides the most favorable results in terms of improving the thermophysical properties of PCMs among metal oxide nanoparticles.

The experimental study consists of two parts: the preparation and characterization of nano-enhanced PCMs, and the testing of the prepared nano-PCM composites, including the measurement of thermal conductivity and latent heat. The results are then collected, processed and analyzed. The final section of the study focuses on the analysis and discussion of the applicability of enhanced PCMs in cold climate regions.

The novelty of this work lies in testing these materials under extreme outdoor conditions, providing valuable

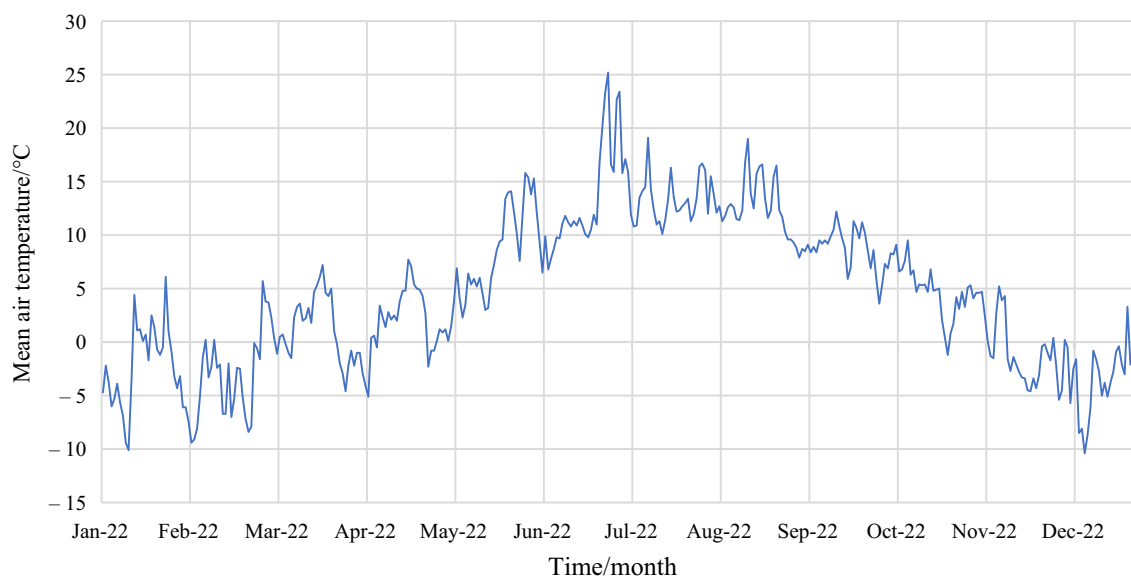


Fig. 1 Air temperature trend in Narvik (NO) [17]

insights into how nano-enhanced PCMs can be modified and integrated into buildings as passive components in energy-demanding cold regions. By varying the melting temperatures of PCMs and nanoparticle concentrations, this study examines the degree of improvement in the thermophysical properties of modified PCMs compared to pure PCMs, evaluating and highlighting their effects and limitations in building applications in cold climates.

## Materials and methods

### Materials

The base PCM used in the study is commercial pure paraffin produced by Rubitherm GmbH. In particular, three products—namely RT10HC, RT15 and RT18HC—are chosen for being modified and tested. These paraffins are identified in the catalog by three distinct melting temperatures—10, 15 and 18 °C, respectively—with their main physical properties outlined in Table 1. Titanium oxide (TiO<sub>2</sub>)—produced by Sigma-Aldrich—serves as nanoparticle, and it is used for modifying the paraffin during the study. This nanofiller is characterized by a particle size smaller than 25 nm and a molecular weight of 79.87 g mol<sup>-1</sup> [18].

A surfactant is also employed to prevent cluster formations during samples preparation. For instance, surfactants are organic molecules able to modify nanoparticles' surface properties providing more stability to the paraffin-TiO<sub>2</sub> mixture [19]. As their performance changes according to the type of PCM and nanoparticles they are combined with, in the first step of the study three different types of surfactants—sodium dodecylbenzene sulfonate (SDBS), sodium dodecyl sulfate (SDS) and hexadecyltrimethylammonium bromide (CTAB), produced by Sigma-Aldrich—are tested, and only one is selected for the following experiments.

**Table 1** Paraffin physical properties [20]

| Product | Melting temperature range/°C | Melting temperature peak/°C | Thermal conductivity/W m <sup>-1</sup> K <sup>-1</sup> | Latent heat/kJ kg <sup>-1</sup> |
|---------|------------------------------|-----------------------------|--|---------------------------------|
| RT10HC  | 9–10                         | 9                           | 0.2  | 200                             |
| RT15    | 10–17                        | 14                          | 0.2  | 155                             |
| RT18HC  | 17–19                        | 18                          | 0.2  | 260                             |

**Table 2** Samples' surfactant, nanoparticles and paraffin concentrations

| Sample | Surfactant | PCM <sub>mass</sub> | TiO <sub>2conc</sub> | TiO <sub>2mass</sub> | Surfactant <sub>conc</sub> | Surfactant <sub>mass</sub> |
|--------|------------|---------------------|----------------------|----------------------|----------------------------|----------------------------|
| Nr. 1  | SDBS       | 15                  | 0.5                  | 0.075                | 25                         | 0.01875                    |
| Nr. 2  | SDS        | 15                  | 0.5                  | 0.075                | 25                         | 0.01875                    |
| Nr. 3  | CTAB       | 15                  | 0.5                  | 0.075                | 25                         | 0.01875                    |

### Surfactant selection and samples' preparation

As introduced in previously, the preliminary step of the study is to identify the surfactant providing the greater stability to the paraffin-TiO<sub>2</sub> samples. Therefore, SDBS, SDS and CTAB are combined with the same type of paraffin—RT10 in this case—and titanium oxide in three different probes, according to quantities and concentrations listed in Table 2. In particular, the mass of nanoparticles and surfactants to use in the solution are calculated as follows:

$$\text{TiO}_{2\text{mass}} = \text{PCM}_{\text{mass}} * \text{TiO}_{2\text{conc}} \quad (1)$$

$$\text{Surfactant}_{\text{mass}} = \text{TiO}_{2\text{mass}} * \text{surfactant}_{\text{conc}} \quad (2)$$

where PCM<sub>mass</sub> [g], TiO<sub>2mass</sub> [g] and Surfactant<sub>mass</sub> [g] are the mass of the paraffin, titanium oxide and surfactant, while TiO<sub>2conc</sub> [%] and surfactant<sub>conc</sub> [%] are the mass percentage of the titanium oxide and the surfactant, respectively.

Samples were prepared using a two-step method—involving stirring and sonication techniques—and carrying out the following procedure. To begin with, paraffin, nanoparticles and surfactants were weighted using a Shimadzu balance and according to quantities shown in Table 2. Then, the beaker containing paraffin was placed inside a fume cupboard over a hot plate of a magnetic stirring. This instrument was set at a velocity of 450 rpm and at a temperature of 30 °C to keep the paraffin in a liquid form. After that, titanium oxide particles were poured slowly and carefully into the paraffin's beaker in order to facilitate a uniform dispersion of the particles and avoid cluster formation. Once the particles were dispersed homogeneously, surfactant was also added in the same way and the whole solution was left stirring for ninety minutes. The beaker was then transferred from the fume cupboard and to the ultrasonic cell disintegrator where the solution was sonicated for thirty minutes. The equipment was set at the sonication amplitude of 40% and a time of 3 s ON and 2 s OFF in order to get a uniform dispersal of nanofillers and surfactants in the base PCM. Finally, the resulted solution was poured into a test tube and placed in a water bath for twelve hours at a constant temperature of 35 °C. Once the procedure was completed, the surfactant was selected.

Therefore, in the following step of the study, new samples were prepared—replicating the same procedure described in this section—combining paraffin, titanium

oxide and the selected surfactant according to quantities reported in Table 3, for a total of twelve PCMs–nanoparticle combinations.

### Thermal conductivity test

To measure thermal conductivity, the twelve prepared samples plus three probes containing pure-paraffin—one for each type—were undergone under the same test procedure, and results were compared. The employed instrument was machine equipped with a heating and cooling system that kept the sample temperature at the desired value. Samples were placed inside the equipment by using a sample holder (Fig. 2a)—designed for this purpose by Muhammad Hayat—consisting of a hollow cylinder

containing the liquid sample in contact with a sensor for data acquisition. The whole system was then connected to a data acquisition system, which collected information through the software Hot Disk Thermal Analyzer. After calibrating the machine—using stainless steel as reference material—thermal conductivity was measured to the following steps. First, the water temperature of the cooling and heating bath (Fig. 2b) was set at the desired temperature. This value can be found in Table 4, and it was chosen according to the temperature of the sample at which the thermal conductivity was to be measured. Indeed, once the sample and the water both reach the setup temperature, the software was run using the heating power and the measurement time listed in Table 4.

**Table 3** Samples' paraffin and nanoparticles quantities

| Sample's number | PCM type | PCM <sub>mass</sub> | TiO <sub>2conc</sub> | TiO <sub>2mass</sub> | Surfactant <sub>conc</sub> | Surfactant <sub>mass</sub> |
|-----------------|----------|---------------------|----------------------|----------------------|----------------------------|----------------------------|
| 1               | RT10 HC  | 15                  | 0.05                 | 0.0075               | 25                         | 0.001875                   |
| 2               |          |                     | 0.1                  | 0.015                |                            | 0.00375                    |
| 3               |          |                     | 0.2                  | 0.03                 |                            | 0.0075                     |
| 4               |          |                     | 0.5                  | 0.075                |                            | 0.01875                    |
| 5               | RT15     | 15                  | 0.05                 | 0.0075               | 25                         | 0.001875                   |
| 6               |          |                     | 0.1                  | 0.015                |                            | 0.00375                    |
| 7               |          |                     | 0.2                  | 0.03                 |                            | 0.0075                     |
| 8               |          |                     | 0.5                  | 0.075                |                            | 0.01875                    |
| 9               | RT18 HC  | 15                  | 0.05                 | 0.0075               | 25                         | 0.001875                   |
| 10              |          |                     | 0.1                  | 0.015                |                            | 0.00375                    |
| 11              |          |                     | 0.2                  | 0.03                 |                            | 0.0075                     |
| 12              |          |                     | 0.5                  | 0.075                |                            | 0.01875                    |

**Fig. 2** **a** Sample holder containing sensor, **b** sample holder containing sample in thermal bath

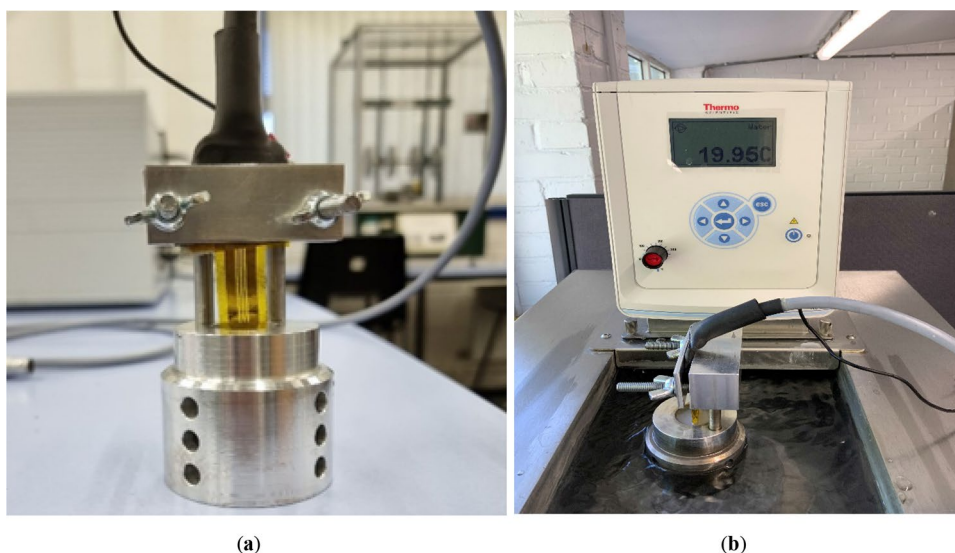


**Table 4** Thermal conductivity setup values

| Parameter                          | Set value |
|------------------------------------|-----------|
| Heating power                      | 80 mW     |
| Measurement time                   | 2 s       |
| Water bath temperature for RT10 HC | 12 °C     |
| Water bath temperature for RT15    | 17 °C     |
| Water bath temperature for RT18 HC | 20 °C     |

For each sample, the test is run three times. The final thermal conductivity value is computed automatically by the software by calculating the weighted average of the three measured values.

### Latent heat test

Latent heat was measured using a differential scanning calorimetry (DSC) (Fig. 3a), a machine used for computing and collect data on samples' melting and solidification temperatures during their charging and discharging phases. The machine was first calibrated taking indium as a reference material. After that, a drop of sample was poured into the small aluminum cylinder shown in Fig. 3b, which was sealed before being inserted into the DSC machine. The minimum and the maximum temperature values set for the measurements were, respectively,  $-20$  and  $25$  °C, corresponding to the temperature range of the arctic environment during the year—see Fig. 1. The temperature ramp was set at  $1$  °C  $\text{min}^{-1}$  as shown in the setup values table (Table 5).

The test was run once for each of the twelve nano-modified paraffins and once also for the three pure paraffin samples.

**Table 5** Latent heat setup values

| Parameter                   | Set value                |
|-----------------------------|--------------------------|
| Initial temperature         | $-20$ °C                 |
| Final temperature           | $25$ °C                  |
| Ramp at final temperature   | $1$ °C $\text{min}^{-1}$ |
| Ramp at initial temperature | $1$ °C $\text{min}^{-1}$ |

## Results and discussion

In this section, an in-depth analysis was carried out to investigate the influence of nanoparticles on thermophysical properties of pure paraffin. Moreover, the effects of modified phase change materials on indoor temperature of a building under cold climate conditions are investigated.

### Effects of surfactants

Surfactant was selected once the process described in *Surfactant selection and samples' preparation* section was completed. The image of the three samples after resting for twelve hours in the water bath at constant temperature is shown in Fig. 4. The methodology used to identify the surfactant providing more stability to the solution is the same presented in [22]. For instance, looking at Fig. 4, the presence of titanium oxide precipitates in the test tubes where CTAB and SDS—first and third sample from the left, respectively—were used is very evident. While in the central sample—containing SDBS—the solution appears more uniform. The absence of precipitates indicates a good interaction of SDBS with the nanoparticles and thus provides a homogenous dispersion of the nanofillers

**Fig. 3** a DCS machine, b cylinders containing samples



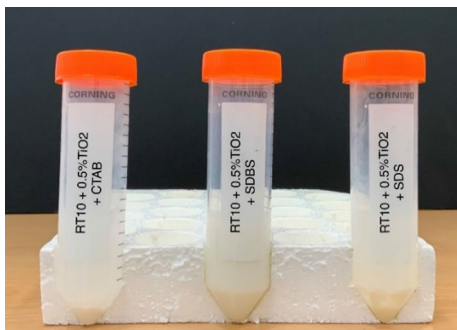


Fig. 4 Surfactant test results

Table 6 Thermal conductivity results

| Additive concentration/mass% | PCM composite conductivity/W m <sup>-1</sup> K <sup>-1</sup> |                        |                        |
|------------------------------|--|------------------------|------------------------|
|                              | RT-10/TiO <sub>2</sub>                                       | RT-15/TiO <sub>2</sub> | RT-18/TiO <sub>2</sub> |
| 0                            | 0.1935   | 0.1902                 | 0.1895                 |
| 0.05                         | 0.2032   | 0.2025                 | 0.1983                 |
| 0.1                          | 0.2193   | 0.2171                 | 0.2155                 |
| 0.2                          | 0.2347   | 0.2343                 | 0.2296                 |
| 0.5                          | 0.2607   | 0.2604                 | 0.2599                 |

from which the whole nano-paraffin solution will benefit. Therefore, the SDBD was chosen as surfactant for all the following twelve prepared samples.

### Effects of nanoparticles concentration on thermal conductivity

The resulted values from the thermal conductivity testing are presented in Table 6. As expected, results clearly indicate the same trend for all the three types of paraffins: increasing the nanoparticle concentration is associated with an increase of the thermal conductivity of the samples. More details are shown in Fig. 5a. The graph highlights that for concentration values of 0.05, 0.1 and 0.2 mass%, RT-15 presents a greater thermal conductivity enhancement—compared to the base-paraffin—than RT-10 and RT-18. Instead, for the concentration of 0.5 mass%, RT-18 shows the higher thermal conductivity increase—compared to the base-paraffin—than RT-10 and RT-15. The percentage increase of thermal conductivity of modified PCMs can be visualized in Fig. 5b, and it has been calculated as follows:

$$\% \text{ increase} = \frac{k_{\text{modified\_PCM}} - k_{\text{base\_PCM}}}{k_{\text{modified\_PCM}}} * 100 \quad (3)$$

where  $k_{\text{modified\_PCM}}$  [W m<sup>-1</sup> K<sup>-1</sup>] is the thermal conductivity of the modified paraffin, while  $k_{\text{base\_PCM}}$  [W m<sup>-1</sup> K<sup>-1</sup>] is the thermal conductivity of the base paraffin.

However, the difference between the different percentage increasing is minimal and—as illustrated in Fig. 5b—comparing paraffins with the same nanoparticle concentrations, it corresponds to a few points percentage. Even though these results were predictable, it is still interesting to show and highlight these outcomes, because the rate of energy stored and released by phase change materials is strictly related to thermal conductivity.

### Effects of nanoparticles concentration on latent heat

Results from differential scanning calorimeter tests are shown in Figs. 6–8. The graphs are based upon three base-PCMs and illustrate the heat flux going through materials during charging—in the negative quadrant—and discharging phases—in the positive quadrant—in function of the temperature. Outcomes highlight that—for each PCM-group—curves of modified paraffins show the same trend and shape as those of the reference-base-paraffin. However, they also show different heat flux peaks in both charging and discharging phases, highlighting that adding nanoparticle leads to an alteration of materials' endothermic and exothermic curves. Indeed, as reported in Tables 7–10, modified PCMs all present a reduced latent heat of melting and cooling values, and in particular, higher the nanoparticle concentration, greater the latent heat difference from pure PCMs.

#### RT10

DSC results from RT10 test are shown in Fig. 6. It can be seen that charging phase occurs within 8 and 12 °C while discharging phase occurs within 8 and 6 °C. Considering the charging phase of the pure PCM, the temperature associated with the heat flux peak was registered at 10.04 °C (see Table 7). Instead, for modified paraffins, the heat flow peak occurs at higher temperature values that increases as increasing the nanoparticle concentration. The heat flow peak value itself also undergoes to a change and a decrease as nanoparticle concentration increases. This behavior is reflected by the decrease of the latent heat of melting, which is 152.5 kJ kg<sup>-1</sup> for pure paraffin and 150.7, 148.7, 147.6 and 143.5 kJ kg<sup>-1</sup> for RT10 with a titanium oxide concentration of 0.05, 0.1, 0.2 and 0.5 mass%, respectively.

On the contrary, during the cooling phase, the behavior is slightly different. The temperature at which the maximum heat flux is reached was registered at 9.02 °C for pure paraffin, while it was occurring at lower temperature values for paraffins with nanoparticle concentrations of 0.05 and 0.1 mass% and at higher temperatures for paraffins with nanoparticle concentrations of 0.2 and 0.5 mass%. The lower

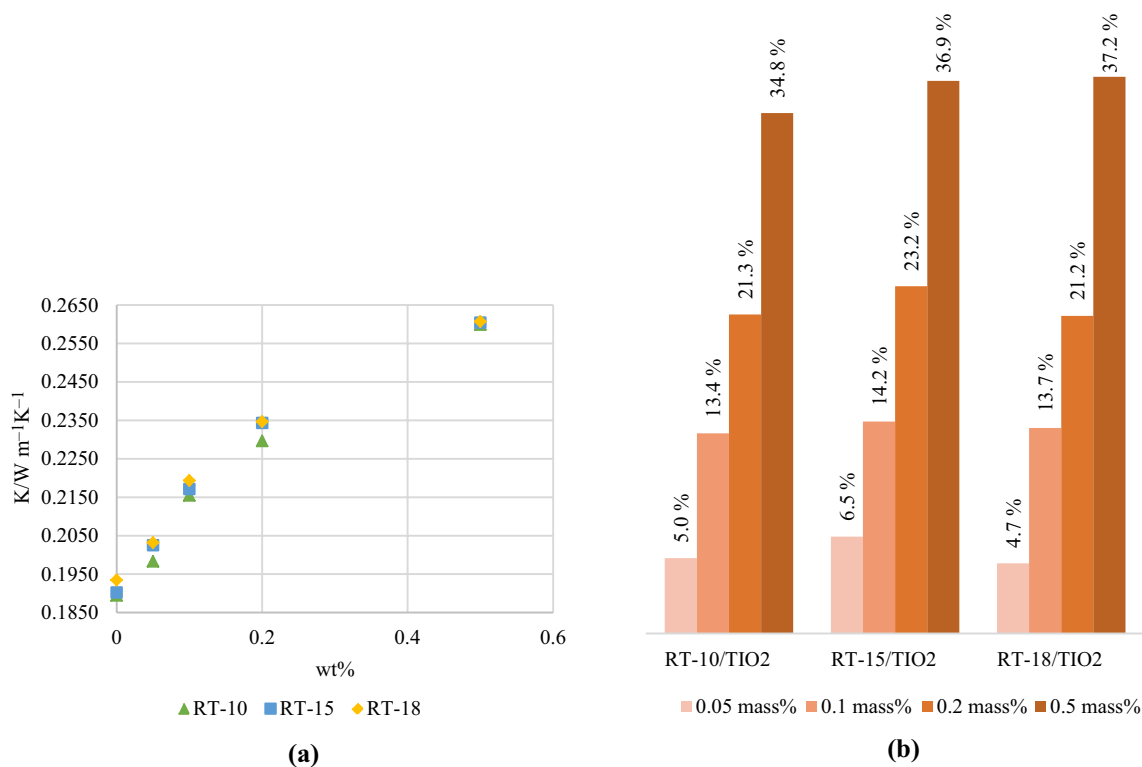
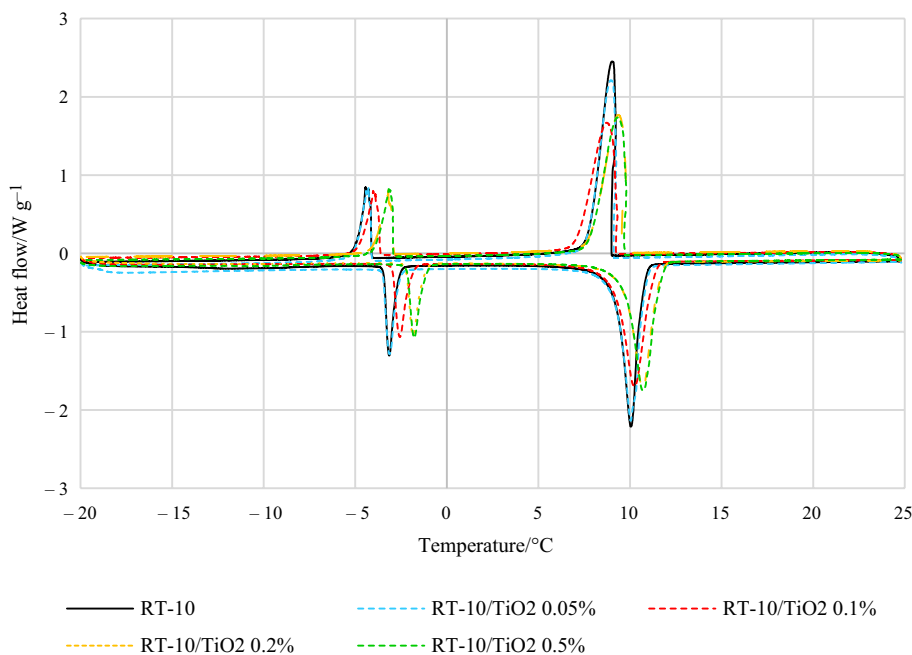


Fig. 5 **a** Thermal conductivity versus TiO<sub>2</sub> concentration values, **b** thermal conductivity percentage raise

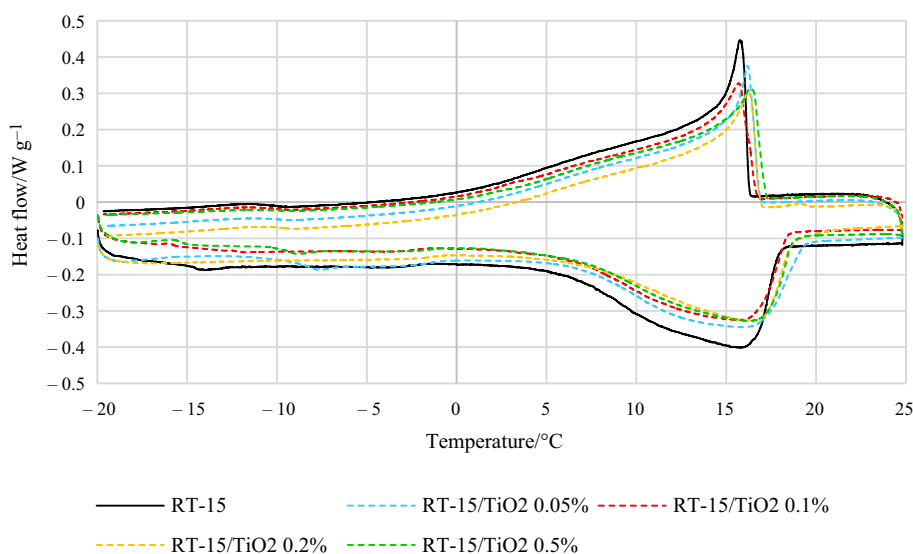
Fig. 6 RT-10 DSC results



heat flow peak is still reflected in the lower values of latent heat of cooling.

The thermographs also highlight another heat flow peak occurring in the temperature interval of - 6 and - 2 °C.

This phenomenon suggests that a solid–solid phase change is occurring [23, 24], whose data are presented in Table 8. During this interval, modified paraffins present the same behavior described before for liquid–solid phase change.

**Fig. 7** RT15 DSC results**Table 7** RT-10 temperature and enthalpy values

| Sample                      | Melting temperature peak/°C | Latent heat of melting /kJ kg <sup>-1</sup> | Cooling temperature peak/°C | Latent heat of cooling /kJ kg <sup>-1</sup> |
|-----------------------------|-----------------------------|---|-----------------------------|---|
| RT-10                       | 10.04                       | 152.5                                       | 9.02                        | 156   |
| RT-10 TiO <sub>2</sub> 0.05 | 10.04                       | 150.7                                       | 8.97                        | 150.7                                       |
| RT-10 TiO <sub>2</sub> 0.1  | 10.27                       | 148.7                                       | 8.74                        | 147.7                                       |
| RT-10 TiO <sub>2</sub> 0.2  | 10.7                        | 147.6                                       | 9.37                        | 146.1                                       |
| RT-10 TiO <sub>2</sub> 0.5  | 10.7                        | 143.5                                       | 9.31                        | 142.3                                       |

## RT15

DSC results from RT15 samples' tests are shown in Fig. 7, and data are presented in Table 9. Curves present a trend that differs from the one analyzed in the previous section. For instance, RT15 curves are characterized by only one peak, occurring during the solid–liquid phase change in the temperature range between 5 and 18 °C. Therefore, the phase change is taking place over a wider temperature interval than the RT10 case. As shown in Table 9, the temperature at which the heat flux peak occurs—during charging phase—is registered at 15.73 °C for the pure paraffin and it becomes higher at a higher nanoparticle concentration. Similarly, during the discharging phase, the temperature at which the heat flux peak occurs, it is measured 15.77 °C for the pure paraffin and at higher temperatures values as increasing nanoparticle concentration.

## RT18

DSC results from RT18 samples' tests are shown in Fig. 8, and data are presented in Table 10. In this case, the

**Table 8** Solid–solid phase change melting and cooling temperature peaks

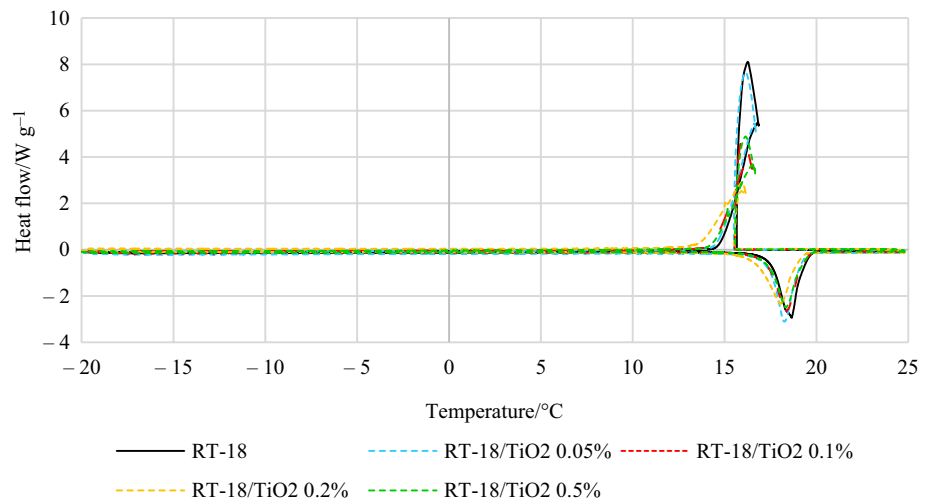
| Sample                      | Melting temperature peak/°C | Cooling temperature peak/°C |
|-----------------------------|-----------------------------|-----------------------------|
| RT-10                       | - 3.44                      | - 4.45                      |
| RT-10 TiO <sub>2</sub> 0.05 | - 3.5                       | - 4.27                      |
| RT-10 TiO <sub>2</sub> 0.1  | - 2.97                      | - 4.03                      |
| RT-10 TiO <sub>2</sub> 0.2  | - 2.22                      | - 3.19                      |
| RT-10 TiO <sub>2</sub> 0.5  | - 2.16                      | - 3.18                      |

solid–liquid phase change occurs during a short interval within 16 and 20 °C, while a liquid–solid phase change within 17 and 15 °C. As the previous cases, latent heat of melting and cooling of the modified PCMs decreases as increasing the titanium oxide concentration as reflection of the lower heat flux peak values registered in these cases.

Finally, Table 11 highlights the percentage reduction of latent heat of melting and cooling for each case mentioned above compared to pure paraffin. The percentage reduction is calculated as follows:



**Fig. 8** RT-18 DSC results



$$\% \text{ decrease} = \frac{H_{\text{base\_PCM}} - H_{\text{modified\_PCM}}}{H_{\text{base\_PCM}}} * 100 \quad (4)$$

where  $H_{\text{modified\_PCM}}$  [kJ kg<sup>-1</sup>] is the latent heat of the modified paraffin, while  $H_{\text{base\_PCM}}$  [kJ kg<sup>-1</sup>] is the latent heat of the base paraffin.

During the charging phase, for nanoparticle concentrations of 0.05 mass% and 0.1 mass%, RT18 shows the smallest percentage decrease compared with other paraffins. While, for the nanoparticle concentrations of 0.2 and 0.5 mass%, RT10 presents the smallest percentage decrease compared with other paraffins. Instead, in the discharging phase, RT18 shows the smallest percentage decrease at any

nanoparticle concentration compared to other modified PCMs.

It is important to highlight these results, because along with thermal conductivity, latent heat affects the performance of phase change materials and their capacity to store and release heat. For instance, a greater decreasing corresponds to a lower capacity of storing and releasing heat—a reflection of a lower heat flux as seen in Figs. 6, 7 and 8.

### Effect of modified PCMs on indoor temperature

In order to understand the benefits of nano-PCMs for the building sector and hence explore their applicability in cold

**Table 9** RT-15 temperatures and enthalpies values

| Sample                      | Melting temperature peak/°C | Latent heat of melting /kJ kg <sup>-1</sup> | Cooling temperature peak/°C | Latent heat of cooling /kJ kg <sup>-1</sup> |
|-----------------------------|-----------------------------|---|-----------------------------|---|
| RT-15                       | 15.73                       | 149.8                                       | 15.77                       | 151.5                                       |
| RT-15 TiO <sub>2</sub> 0.05 | 16.18                       | 148.8                                       | 16.21                       | 147.4                                       |
| RT-15 TiO <sub>2</sub> 0.1  | 15.87                       | 141.3                                       | 15.68                       | 142.3                                       |
| RT-15 TiO <sub>2</sub> 0.2  | 16.49                       | 139.7                                       | 16.26                       | 137.4                                       |
| RT-15 TiO <sub>2</sub> 0.5  | 16.26                       | 130.5                                       | 16.34                       | 133.8                                       |

**Table 10** RT-18 temperature and enthalpies values

| Sample                      | Melting temperature peak/°C | Latent heat of melting /kJ kg <sup>-1</sup> | Cooling temperature peak/°C | Latent heat of cooling /kJ kg <sup>-1</sup> |
|-----------------------------|-----------------------------|---|-----------------------------|---|
| RT-18                       | 18.65                       | 240.4                                       | 16.24                       | 242.8                                       |
| RT-18 TiO <sub>2</sub> 0.05 | 18.25                       | 239.1                                       | 16.07                       | 239.9                                       |
| RT-18 TiO <sub>2</sub> 0.1  | 18.35                       | 236.7                                       | 16.06                       | 232.9                                       |
| RT-18 TiO <sub>2</sub> 0.2  | 18.04                       | 231.7                                       | 15.95                       | 229.2                                       |
| RT-18 TiO <sub>2</sub> 0.5  | 18.33                       | 219.1                                       | 16.11                       | 221.7                                       |

**Table 11** Latent heat of melting and cooling percentage decrease

| Sample                      | Latent heat of melting /kJ kg <sup>-1</sup> | Latent heat of melting percentage decrease/% | Latent heat of cooling /kJ kg <sup>-1</sup> | Latent heat of cooling percentage decrease/% |
|-----------------------------|---|--|---|--|
| RT-10                       | 152.5                                       | 0  | 156   | 0  |
| RT-10 TiO <sub>2</sub> 0.05 | 150.7                                       | 1.2  | 150.7                                       | 3.4  |
| RT-10 TiO <sub>2</sub> 0.1  | 148.7                                       | 2.5  | 147.7                                       | 5.3  |
| RT-10 TiO <sub>2</sub> 0.2  | 147.6                                       | 3.2  | 146.1                                       | 6.3  |
| RT-10 TiO <sub>2</sub> 0.5  | 143.5                                       | 5.9  | 142.3                                       | 8.8  |
| RT-15                       | 149.8                                       | 0  | 151.5                                       | 0  |
| RT-15 TiO <sub>2</sub> 0.05 | 148.8                                       | 0.7  | 147.4                                       | 2.7  |
| RT-15 TiO <sub>2</sub> 0.1  | 141.3                                       | 5.7  | 142.3                                       | 6.1  |
| RT-15 TiO <sub>2</sub> 0.2  | 139.7                                       | 6.7  | 137.4                                       | 9.3  |
| RT-15 TiO <sub>2</sub> 0.5  | 130.5                                       | 12.9   | 133.8                                       | 11.7   |
| RT-18                       | 240.4                                       | 0  | 242.8                                       | 0  |
| RT-18 TiO <sub>2</sub> 0.05 | 239.1                                       | 0.5  | 239.9                                       | 1.2  |
| RT-18 TiO <sub>2</sub> 0.1  | 236.7                                       | 1.5  | 232.9                                       | 4.1  |
| RT-18 TiO <sub>2</sub> 0.2  | 231.7                                       | 3.6  | 229.2                                       | 5.6  |
| RT-18 TiO <sub>2</sub> 0.5  | 219.1                                       | 8.9  | 221.7                                       | 8.7  |

climate regions, it is necessary to analyze their effect on indoor temperature of residential buildings.

Considering Narvik as reference city—as justified in the Introduction section—and using air temperature data of Fig. 1, the research now compares the charging and discharging temperature ranges of pure and modified PCMs reported in the previous section with the air temperature data taken as reference. Indeed, since test showed similar data for the investigated paraffins, the purpose now it is to highlight the applicability of enhanced PCMs understanding when and in which season they can actually contribute as thermoregulation passive element.

RT10 paraffins showed a charging temperature range within 8 and 12 °C and a discharging phase within 8 and 6 °C. RT15 paraffins showed a wider charging temperature range within 5 °C and 18 °C and a discharging phase within 16 and 5 °C. Lastly, RT18 paraffins showed a charging temperature range within 16 and 18 °C and a discharging phase within 17 and 15 °C. These results indicate that enhanced RT15 can activate—and thus store heat—more often than the other paraffins due to their larger solid–liquid phase change range. However, they show lower values of latent heat of melting and cooling. On the other hand, RT18 presents the best values in terms of latent heat and thermal conductivity—considering both the increase and the value itself—but they are able to phase change only when outdoor conditions reach 16 °C, which—looking at Fig. 1—it happens only during warmest month when there is a little thermoregulation need. Finally enhanced RT10 shows a good compromise between the two previous cases, being able to activate during cold and mild-cold months and with a high latent heat value with small percentage decreases when

added nanoparticles. Hence, RT10-modified paraffins best fit the cold climate condition applications.

The importance of highlights of this outcome is to understand when phase-transition-temperature range matches the outside conditions and hence identify when paraffins can change from solid to liquid storing thermal energy from the outside to release into the building and release it when the outside temperature drops down and their phase changes again from solid to liquid.

## Conclusions

In this study, nano-PCM composites were prepared and compared to pure base PCMs. The thermal properties of the developed composites, such as thermal conductivity and melting and cooling enthalpies, were measured to evaluate the impact of nanoparticles on these pure PCMs. The following conclusions were obtained:

- Three different surfactants were initially tested for PCM preparation evaluation. Under identical concentrations, SDBS exhibited the best stability for the nano-TiO<sub>2</sub>-paraffin composite, showing the least amount of precipitates in the test tube;
- Thermal conductivity tests showed an improvement in the thermal conductivity of base paraffin by 5 and 37% for nano-TiO<sub>2</sub> concentrations of 0.05 mass% and 0.5 mass%, respectively. The increase in thermal conductivity was directly proportional to the nanoparticle concentration in the samples;

- Latent heat tests revealed different behaviors and curves in the tested paraffins. Generally, the addition of nanoparticles led to a decrease in the latent heat of melting. This reduction ranged from 0.5% in the case of RT18 with a 0.05 mass% concentration to 12.9% in the case of RT15 with a 0.5 mass% concentration;
- Among the three tested paraffins, nano-TiO<sub>2</sub> RT10 showed a slightly slower increase in thermal conductivity compared to nano-TiO<sub>2</sub> RT15, but similar values compared to Nano-TiO<sub>2</sub> RT18. It also exhibited the lowest decrease in latent heat of melting and cooling, which is advantageous for heat storage and release in building applications;
- When assessing the applicability of PCMs in the building sector under cold climate conditions, it was found that RT10 is compatible with the arctic temperature range during cold and mild-cold seasons, with an operating melting and cooling temperature range between 5 and 12 °C. As a result, modified RT10 is more suitable for integration into building structures compared to the other two modified paraffins, especially during energy-demanding arctic seasons;

Future research should address several points that have not been extensively covered in this study. For instance, a more in-depth analysis is needed to better understand the potential of the selected enhanced PCMs as passive elements within buildings, including quantifying the effective energy savings and associated costs.

**Acknowledgements** This research was supported by School of Physics, Engineering and Computer Science at the University of Hertfordshire, Hatfield (UK). The publication charges for this article have been funded by a grant from the publication fund of UiT, The Arctic University of Norway.

**Author contributions** All authors contributed to the study conception and design. Material preparation, data collection and analysis were performed by L.R, M.A.H and Y.C. L.R wrote the original draft and curated the data; M.A.H was involved in writing—reviewing and editing, data curation and investigation; Y.C was involved in writing—review and editing, investigation, project administration, supervision, funding acquisition. R.K.C and R.R. were responsible for reviewing and editing, project administration, funding acquisition and supervision.

**Funding** Open access funding provided by UiT The Arctic University of Norway (incl University Hospital of North Norway).

## Declarations

**Conflicts of interest** The authors declare no conflict of interest.

**Open Access** This article is licensed under a Creative Commons Attribution 4.0 International License, which permits use, sharing, adaptation, distribution and reproduction in any medium or format, as long as you give appropriate credit to the original author(s) and the source, provide a link to the Creative Commons licence, and indicate if changes

were made. The images or other third party material in this article are included in the article's Creative Commons licence, unless indicated otherwise in a credit line to the material. If material is not included in the article's Creative Commons licence and your intended use is not permitted by statutory regulation or exceeds the permitted use, you will need to obtain permission directly from the copyright holder. To view a copy of this licence, visit <http://creativecommons.org/licenses/by/4.0/>.

## References

1. Durakovic B. Pcm-based building envelope systems: innovative energy solutions for passive design; Cham: Springer; 2020. pp. 1–16.
2. Alva G, Lin Y. An overview of thermal energy storage systems. *Energy J.* 2018;81:1771–86.
3. Hayat MA, Chen Y. Characteristics and potential applications of nano-enhanced phase change materials: Aa critical review on recent development. *Sustain Energy Technol Assess.* 2021;50:101–799.
4. Teng TP, Yu CC. Characteristics of phase-change materials containing oxide nano-additives for thermal storage. *Nanoscale Res Lett.* 2021;7:611.
5. Kim S, Drzal LT. High latent heat storage and high thermal conductive phase change materials using exfoliated graphite nanoplatelets. *Sol Energy Mater Sol Cells.* 2009;93:136–42.
6. Putra N, Amin MN. Characterization of the thermal stability of RT 22 HC/graphene using a thermal cycle method based on thermoelectric methods. *Appl Therm Eng.* 2017;124:62–70.
7. Fan L-W, Fang X. Effects of various carbon nanofillers on the thermal conductivity and energy storage properties of paraffin-based nanocomposite phase change materials. *Appl Energy.* 2013;110:163–72.
8. Wang J, Xie H. Improved thermal properties of paraffin wax by the addition of TiO<sub>2</sub> nanoparticles. *Appl Therm Eng.* 2014;73:1541–7.
9. Zhang G, Yu Z. Fabrication of a novel nano phase change material emulsion with low supercooling and enhanced thermal conductivity. *Renew Energy.* 2020;151:542–50.
10. Sami S, Etesami N. Improving thermal characteristics and stability of phase change material containing TiO<sub>2</sub> nanoparticles after thermal cycles for energy storage. *Appl Therm Eng.* 2017;124:346–52.
11. Babapoor A, Karimi G. Thermal properties measurement and heat storage analysis of paraffin and nanoparticles composites phase change material: comparison and optimization. *Appl Therm Eng.* 2015;90:945–51.
12. Liu L, Yang Yan KZ. Graphene aerogels enhanced phase change materials prepared by one-pot method with high thermal conductivity and large latent energy storage. *Sol Energy Mater Sol Cells.* 2018;185:487–93.
13. Mingzheng Z, Guodong X. Analysis of factors influencing thermal conductivity and viscosity in different kinds of surfactant solutions. *Exp Therm Fluid Sci.* 2012;36:22–9.
14. Meng X, Zhang H. Preparation and thermal properties of fatty acids/CNTs composite as shape-stabilized phase change materials. *J Therm Anal.* 2012;111:377–84.
15. Harish S, Orejón D. Thermal conductivity enhancement of lauric acid phase change nanocomposite with graphene nanoplatelets. *Appl Therm Eng.* 2015;80:205–11.
16. Planning and Building Act. <https://www.regjeringen.no/en/dokumenter/planning-building-act/id570450/>. Accessed 25 May 2023.

17. Yr.no. <https://www.yr.no/nb/historikk/graf/5-84701/Norge/Nordland/Narvik/Narvik?q=2022>. Accessed 25 May 2023.
18. Sigma-Aldrich. <https://www.sigmaaldrich.com>. Accessed 3 Dec 2022.
19. Zheng L, Zheng W. Experimental studies of phase change and microencapsulated phase change materials in a cold storage/transportation system with solar driven cooling cycle. *Energies*. 2017;10:1867.
20. Rubitherm, PCM RT-LINE. <https://www.rubitherm.eu/en/productcategory/organische-pcm-rt>. Accessed 19 Dec 2022.
21. Sigma-Aldrich. <https://www.sigmaaldrich.com/NO/en/sds/aldrich/637254>. Accessed 19 Dec 2022.
22. Hayat MA, Chen Y. Preparation and thermophysical characterization analysis of potential nano-phase transition materials for thermal energy storage applications. *J Mol Liq*. 2023;376:121464.
23. Taggart AM, Voogt F. An examination of the nucleation kinetics of n-alkanes in the homologous series C<sub>13</sub>H<sub>28</sub> to C<sub>32</sub>H<sub>66</sub>, and their relationship to structural type, associated with crystallization from stagnant melts. *Langmuir J*. 1996;23:5722–8.
24. Oliver MJ, Calvert PD. Homogeneous nucleation of n-alkanes measured by differential scanning calorimetry. *J Cryst Growth*. 1975;30:137–45.

**Publisher's Note** Springer Nature remains neutral with regard to jurisdictional claims in published maps and institutional affiliations.